JOURNAL OF GENERAL VIROLOGY

RESEARCH ARTICLE

Lipovsky *et al.*, *Journal of General Virology* 2017;98:2821–2836

DOI 10.1099/jgv.0.000954

MICROBIOLOGY SOCIETY

The cellular endosomal protein stannin inhibits intracellular trafficking of human papillomavirus during virus entry

Alex Lipovsky,[1]† Asu Erden,[1]† Eriko Kanaya,[1] Wei Zhang,[2] Mac Crite,[3] Clinton Bradfield,[4] John MacMicking,[4,5] Daniel DiMaio,[2,6,*] John W. Schoggins[7] and Akiko Iwasaki[1,5,6,*]

Abstract

Human papillomaviruses (HPVs) are the most common sexually transmitted viruses and one of the most important infectious causes of cancers worldwide. While prophylactic vaccines are effective against certain strains of HPV, established infections still cause deadly cancers in both men and women. HPV traffics to the nucleus via the retrograde transport pathway, but the mechanism of intracellular transport of non-enveloped viruses such as HPV is incompletely understood. Using an overexpression screen, we identify several genes that control HPV16 entry. We focused on the mechanism by which one of the screen hits, stannin, blocks HPV16 infection. Stannin has not been previously implicated in virus entry. Overexpression of stannin specifically inhibits infection by several HPV types, but not other viruses tested. Stannin is constitutively expressed in human keratinocytes, and its basal levels limit entry by HPV16. Stannin is localized to the endolysosomal compartment and does not affect HPV16 binding to cells, virus uptake, or virus uncoating, but inhibits the entry of HPV into the trans-Golgi network (TGN) and stimulates HPV degradation. We further show that stannin interacts with L1 major capsid protein and impairs the interaction of the L2 minor capsid protein with retromer, which is required for virus trafficking to the TGN. Our findings shed light on a novel cellular protein that interferes with HPV entry and highlight the role of retrograde transport in HPV entry.

INTRODUCTION

Human papillomaviruses (HPVs) are small DNA tumour viruses responsible for 5 % of all cancers worldwide [1]. Among them, HPV16 is linked to 50 % of all cervical cancers and a large fraction of anogenital and oropharyngeal malignancies [2]. HPVs are non-enveloped viruses consisting of a double-stranded DNA viral genome encapsidated by the major capsid protein L1, which forms the outer rigid shell of the virion, and the minor capsid protein L2, which plays an essential role in viral intracellular trafficking events during virus entry. HPVs exclusively infect basal keratinocytes of the skin and mucosal epithelium. Entry is initiated by virus binding to plasma membrane heparan sulfate proteoglycans (HSPGs) [3]. This triggers conformational changes in the HPV capsid, followed by proteolytic cleavage of L1 and L2 by kallikrein-8 and furin, respectively [4, 5], transfer to an elusive secondary uptake receptor [6], and endocytosis via a poorly understood mechanism [7]. Capsid disassembly begins in the endosome followed by vesicular retrograde transport of the viral L1/L2/DNA subcomplex to the trans-Golgi network (TGN), Golgi apparatus and endoplasmic reticulum (ER) [8–11]. A role for the multivesicular endosomes in HPV16 trafficking has also been reported [7, 12]. Productive HPV16 infection requires cell cycle progression and nuclear envelope breakdown during mitosis to allow viral DNA to exit the vesicular compartment and enter the nucleus [13–17]. Viral trafficking can be a rapid process if the target cells are infected shortly prior to

Received 13 September 2017; Accepted 6 October 2017

Author affiliations: [1]Department of Immunobiology, Yale School of Medicine, New Haven, CT 06520-8011, P.O. Box 208011, USA; [2]Department of Genetics, Yale School of Medicine, New Haven, CT 06520-8005, P.O. Box 208005, USA; [3]Microbiology Graduate Program, Yale School of Medicine, New Haven, CT 06519, 295 Congress Avenue, USA; [4]Department of Microbial Pathogenesis, Yale School of Medicine, New Haven, CT 06536-0812, P. O. Box 9812, USA; [5]Howard Hughes Medical Institute, Chevy Chase, MD 20814, USA; [6]Yale Cancer Center, New Haven, CT 06520-8028, PO Box 208028, USA; [7]Department of Microbiology, University of Texas Southwestern Medical Center, 5323 Harry hines Blvd., Dallas, TX 75390, USA.
***Correspondence:** Daniel DiMaio, daniel.dimaio@yale.edu; Akiko Iwasaki, akiko.iwasaki@yale.edu

Keywords: viral entry; retrograde transport; retromer; intracellular trafficking.

Abbreviations: AAV2, adeno-associated virus type 2; BSA, bovine serum albumin; CIMPR, cation-independent mannose phosphate receptor; EdU, 5-ethynyl-2′-deoxyuridine; ER, endoplasmic reticulum; HPV, human papillomavirus; HSPGs, heparan sulfate proteoglycans; HSV1, herpes simplex virus type 1; ISG, IFN-stimulated gene; p.i., post-infection; PLA, proximity ligation assay; PSTCD, *Propionibacterium shermanii* transcarboxylase protein domain; PsV, pseudoviruses; *SERPINE1*, serpin E1; *SNN*, stannin; TGN, trans-Golgi network; THBD, thrombomodulin; vge, viral genome equivalents; VMP1, vacuole membrane protein 1.

†These authors contributed equally to this work.

Eight supplementary figures and two supplementary tables are available with the online Supplementary Material.

mitosis [18]. However, since mitotic entry of most cells in culture is not synchronized, HPV is typically internalized over a period of many hours with endosomal, TGN and nuclear localization most apparent after approximately 8, 16 and 24 h, respectively [10, 17]. Viral gene expression is tightly linked to differentiation of host epithelial cells, and viral assembly does not take place until shortly prior to keratinocyte shedding from the uppermost layer of the infected epithelium [19].

Viral cell entry and intracellular trafficking depends on the coordinated activities of numerous cellular proteins [20]. Therefore, identification and characterization of cellular factors that facilitate or inhibit infection provide mechanistic insight into virus entry and the cell biology underlying this complex process. Most studies of the initial stages of HPV infection have utilized HPV pseudoviruses (PsV), which contain L1 and L2 and are structurally similar to authentic virions. HPV PsV do not incorporate the authentic HPV genome [21], but instead contain a reporter gene, which allows ready assessment of infection. Use of HPV PsV also allows the construction and analysis of viral mutants.

Several cellular retrograde trafficking factors and other cellular proteins required for entry have been shown to associate with the L2 protein before the viral DNA reaches the nucleus [22–25]. An important entry factor is the retromer, a cytoplasmic protein complex that typically binds to the cytoplasmic tail of cellular transmembrane protein cargoes at the endosomal membrane and recruits them into transport vesicles that later fuse with the membranes of the TGN [8, 26]. The retromer binds directly to a highly conserved sequence motif in the C-terminus of the L2 protein, and retromer knock-down or mutation of the retromer-binding sites in L2 results in accumulation of the virus in the endosome and inhibits transport to the TGN [22]. Interestingly, the retromer and several other L2-binding partners (e.g. SNX17) are located in the cytoplasm, whereas the incoming virus itself is in the lumen of the endosome. These results suggest that a portion of the L2 protein protrudes through the endosomal membrane into the cytoplasm where it can bind the retromer and other cytoplasmic factors [8, 23, 27]. Recent antibody and protease sensitivity studies showed that much of L2 is in fact accessible at the cytoplasmic face of the endosomal membrane prior to transport to the TGN, apparently anchored into the membrane by a putative N-terminal transmembrane domain in L2 [27, 28]. This membrane penetration event may be mediated by a membrane-destabilizing sequence in the extreme C-terminus of the L2 protein near the retromer-binding sites [29].

To identify additional cellular factors involved in HPV infection, we conducted an overexpression genetic screen using a library of IFN-stimulated genes (ISGs) [30]. IFNs are potent antiviral cytokines that block virus infection and replication by inducing hundreds of ISGs with direct antiviral activity [31]. Treatment of human keratinocytes with exogenous IFNs inhibits HPV16 infection [32–34]. Our screen identified a unique set of genes that affect HPV16 PsV infection, most of which have not been previously implicated in infection by viruses. One of the top hits in the screen, stannin, inhibits infection by several HPV PsV types but does not appear to be IFN-inducible in our system. We discovered that stannin binds to the HPV capsid during infection and inhibits proper intracellular trafficking of HPV16 to the TGN. Our report identifies a cellular protein that can inhibit infection by HPVs and provides additional insight into the molecular machinery and processes that control retrograde trafficking of HPV during virus entry.

RESULTS

Genetic overexpression screen identifies a unique set of genes involved in inhibition of HPV16 infection

To identify host genes that control HPV16 entry, we used HeLa cervical carcinoma cells, which are amenable to lentiviral transduction and are susceptible to HPV16 infection. The cells were screened for HPV16 PsV reporter gene expression as described previously using a high-throughput flow cytometry-based platform [30]. HeLa cells were seeded into 96-well plates and transduced in a one gene per well format with an arrayed lentiviral cDNA library expressing 387 ISGs. Since the lentiviral vector co-expresses a bicistronic ISG-IRES-TagTagRFP cassette, efficiency of transduction was monitored by RFP expression. Transduced cells were infected with HPV16 PsV incorporating a GFP reporter plasmid (HPV16-GFP), produced as described previously [21]. Two days after infection, the cells were assayed by flow cytometry for RFP and GFP fluorescence (Fig. 1a). Our screens achieved an average lentivirus transduction efficiency of >50 %. Poor transduction (<10 % RFP + cells) was observed for 40 genes and only four ISGs were found to be cytotoxic (resulting in <50 % of the control cell number) (Table S1, available in the online Supplementary Material). The majority of the ISGs had a minor effect on HPV16 PsV entry as assessed by GFP expression ($-1<Z<1$). However, a handful of ISGs were found to strongly inhibit ($Z<-2$) or potentiate ($Z>2$) PsV infection (Fig. 1b). There was excellent reproducibility between two independent screen replicates for both the top inhibitors and the top enhancers of HPV16 PsV infection (Fig. 1b).

Top screen hits specifically control infection of multiple HPV types

None of the top hits identified in the genetic screen were previously implicated in HPV16 infection. We validated a subset of genes with the strongest inhibitory activity, including *SNN* (stannin), *THBD* (thrombomodulin), *SERPINE1* (serpin E1) and *VMP1* (vacuole membrane protein 1). Other than *SERPINE1*, previously reported to have activity against influenza virus [35], none of the other top hits have known antiviral activities. To ensure that the screen findings were not due to a cell line-specific artifact, we validated the top inhibitory hits in HaCaT cells, a human skin keratinocyte cell line. Lentiviral transduction of HaCaT cells led to target gene overexpression at the mRNA level (Fig. S1).

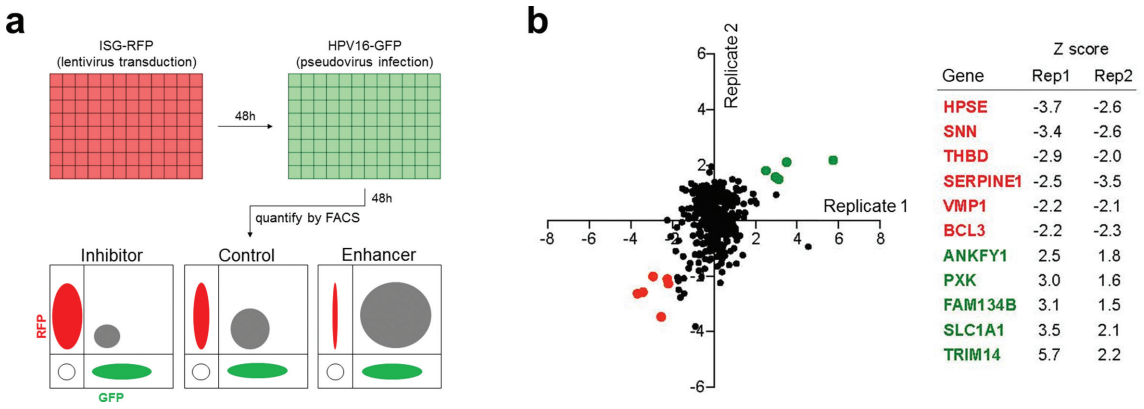

Fig. 1. ISG screen identifies human genes that restrict HPV16 entry. (a) Schematic diagram of the flow cytometry-based overexpression screen. Top two panels show 96-well plates of HeLa cells sequentially infected with ISG lentiviruses expressing RFP and HPV16 pseudovirus expressing GFP. Hypothetical flow cytometry plots of ISGs that inhibit or enhance HPV16-GFP PsV infection are shown at the bottom. GFP$^+$TagRFP$^+$ cells are depicted as grey. (b) Distribution of Z score values for the two replicates of the ISG screen. Each spot represents a single ISG. Top hits are highlighted with red (inhibitors) or green (potentiators). Table lists top hits with Z score for both replicates.

HPV16-GFP infection was inhibited by overexpression of *SNN*, *THBD* and *VMP1*, but not *SERPINE1* in HaCaT cells (Fig. 2a). In contrast, infection with adenovirus, an unrelated small, non-enveloped double-stranded DNA virus, was not significantly affected by any of the tested genes (Fig. 2b). To evaluate the ability of *SNN*, *THBD* and *VMP1* to inhibit entry by other oncogenic HPV types, we infected the corresponding overexpressing cell lines with HPV5 and HPV18 PsVs. HPV5 and HPV18 are linked to skin and cervical cancer, respectively [1, 36]. *SNN*, *THBD* and *VMP1* overexpression inhibited HPV5-GFP and HPV18-GFP infection to a similar extent as HPV16-GFP (Fig. 2b). In addition, *SNN* overexpression did not inhibit infection by JC polyomavirus, herpes simplex virus type 1 (HSV1), or adeno-associated virus type 2 (AAV2) (Fig. 2c). Inhibition of infection by multiple HPV types, but not other tested viruses, suggests that these genes specifically inhibit HPV infection, as opposed to disrupting essential cellular processes or acting as pan-antiviral factors.

Genetic deletion of stannin promotes HPV16 infection

Stannin, an 88-residue transmembrane protein encoded by the *SNN* gene, was one of the strongest inhibitors identified, leading to an approximately three and fivefold inhibition of HPV16-GFP infection in HaCaT and HeLa cells, respectively. We therefore focused on studying the role played by stannin during HPV16 entry. We first determined the effect of basal *SNN* expression on HPV16 infection efficiency by using CRISPR-Cas9 genome editing. HeLa cells were transduced with three lentiviral vectors each encoding Cas9 as well as a guide RNA specific for a unique sequence within the *SNN* genomic locus (see Methods). We were unable to confirm *SNN* mutagenesis by Western blotting because endogenous stannin protein levels could not be detected with the available antibodies. Therefore, we screened clonal cell lines for the presence of deletions within the *SNN* locus by PCR and identified three independent clonal cell lines lacking full-length *SNN* (Fig. S2). All three cell lines expressed reduced levels of *SNN* mRNA (Fig. 2d). Notably, HPV16-GFP PsV infection efficiency was increased by more than 50 % in all three *SNN* mutant cell lines (Fig. 2d). In contrast, infection by adenovirus and herpes simplex virus was not significantly affected by *SNN* knockout. In one of these cell lines, we showed by DNA sequencing that all *SNN* alleles contain a 69-base pair deletion that removed more than one-quarter of the stannin-coding region, combined in some cases with smaller deletions (Fig. S2). These deletions in *SNN* are predicted to produce short aberrant protein product(s) lacking much or all of the stannin linker region, which we show below is essential for antiviral activity. There results indicate that basal levels of stannin inhibit HPV16-GFP infection in HeLa cells.

Stannin is not IFN-inducible in HaCaT cells

Stannin is a highly evolutionarily conserved protein with no homology to known proteins and with poorly understood biological function [37]. Stannin expression in neurons is associated with susceptibility to neurotoxicity induced by trimethyltin [38]. Stannin mRNA and protein are expressed in a wide variety of human tissues, including the squamous epithelial cells of the cervical mucosa [39, 40] – a major *in vivo* target of HPV16 infection. We detected endogenous *SNN* mRNA in all cell types examined, including human primary keratinocytes and peripheral blood mononuclear cells (Fig. S3a). However, treatment of HaCaT cells with recombinant IFN-β, IFN-κ or IFN-γ did not upregulate *SNN* mRNA expression, despite inducing a robust increase in the mRNA levels for bona fide ISGs such as *Mx1* (Fig. S3b, and data not shown). Thus, *SNN* does not appear to be

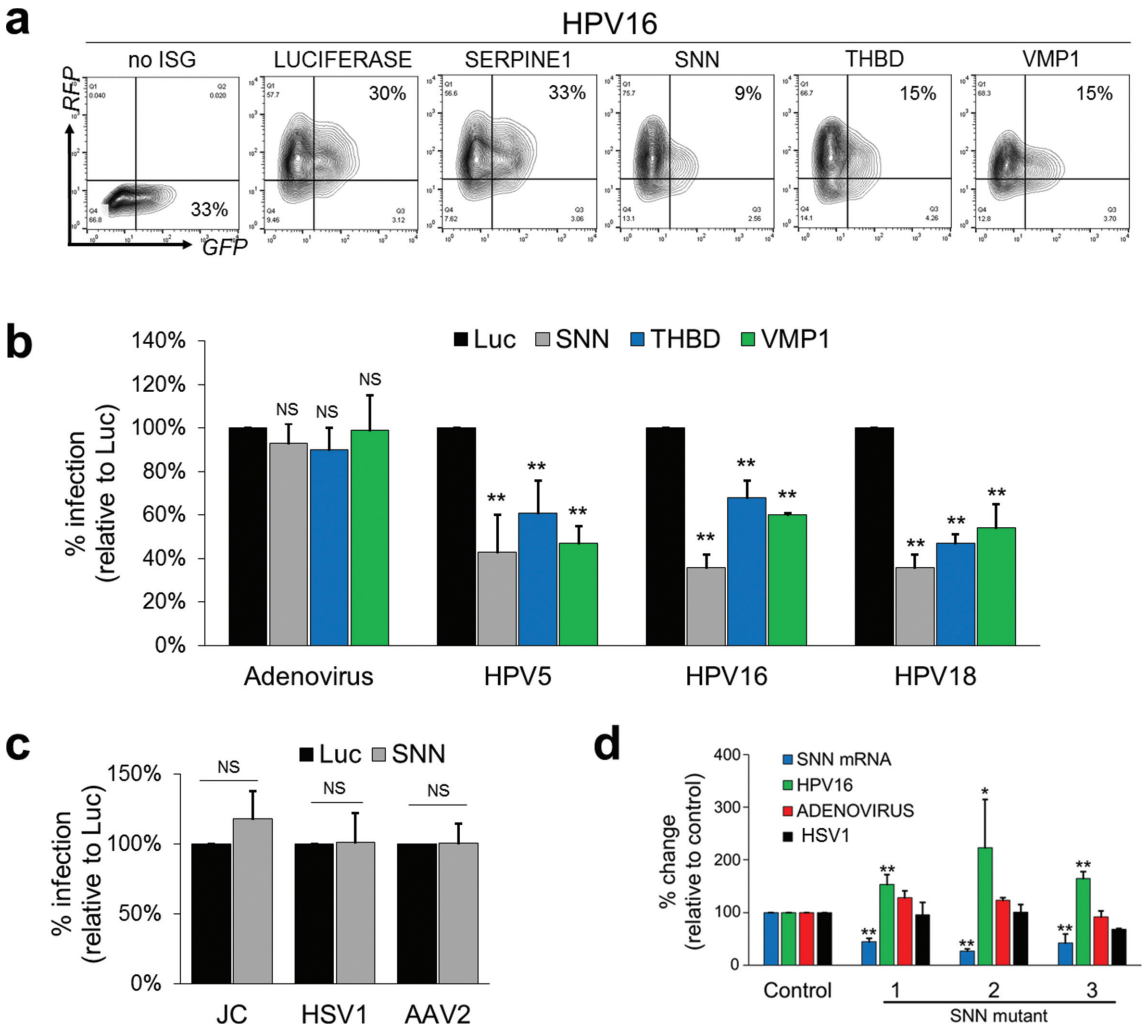

Fig. 2. Validation of top inhibitory ISG screen hits in HaCaT cells. (a, b) Unmodified HaCaT cells (no ISG) or cells stably overexpressing *Luciferase* control, *SERPINE1*, *SNN*, *THBD* or *VMP1* were infected with HPV5-GFP [3×10^4 viral genome equivalents (vge) cell^{-1}], HPV16-GFP ($0.5-1\times10^3$ vge cell^{-1}), HPV18-GFP (3×10^3 vge cell^{-1}) or adenovirus5-GFP (2×10^2 vge cell^{-1}). GFP expression was assayed by flow cytometry 48 h (HPV) or 36 h (adenovirus) later. (a) Representative flow cytometry plots of cells infected with HPV16-GFP. (b) Infection efficiency of adenovirus, HPV5-GFP, HPV16-GFP and HPV18-GFP in cells transduced with the indicated ISG, normalized to infection in control cells expressing luciferase (luc). (c) HaCaT cells stably overexpressing *Luciferase* (black bars) or *SNN* (grey bars) were infected with HSV1-GFP (m.o.i.=0.25), JCV-GFP (5×10^4 vge cell^{-1}) or AAV2-GFP (5×10^4 vge cell^{-1}), and GFP expression assayed by flow cytometry after 24 h (HSV1 and AAV2) or 48 h (JC). (d) The *SNN* genomic locus in HeLa cells was edited with the CRISPR Cas9 system as described in Methods. Control unedited cells and three clones of *SNN* knockout cells were incubated with 50–100 vge cell^{-1} of HPV16-GFP PsV, 50 vge cell^{-1} of adenovirus5-GFP, or HSV1-GFP and assayed for *SNN* mRNA expression (blue bars) and for GFP expression by flow cytometry 48 h (HPV), 36 h (adenovirus), or 24 h (HSV1) later. For (b–d), results show the mean and SD from three independent experiments. Where indicated, statistical significance was determined by ANOVA (b) or an unpaired two-tailed *t*-test (c, d): **P*<0.05; ***P*<0.01. NS, not significant.

an ISG in these cells. Therefore, SNN overexpression interferes with HPV entry in a manner independent of IFNs.

Stannin control of HPV16 entry does not rely on autophagy, cell cycle perturbation or inhibition of furin-mediated L2 cleavage

We examined whether stannin-mediated inhibition of HPV required autophagy, an antiviral defence mechanism reported to control HPV16 entry [41, 42]. To investigate this, we generated *ATG5−/−* HeLa cells using the CRISPR Cas9 system. ATG5 is required for the execution of autophagy [43]. Wild-type and *ATG5−/−* HeLa cells were stably transduced with lentiviruses encoding *Luciferase* or *SNN* cDNAs and then infected with HPV16-GFP. HPV16 PsV infection efficiency increased by 50 % in *ATG5−/−* cells compared to unmodified wild-type cells, as expected,

providing evidence that ATG5 knockout impaired autophagy. Overexpression of *SNN* in wild-type and *ATG5−/−* cells led to similar inhibition of HPV16-GFP infection efficiency (Fig. S4a). These results indicated that autophagy is not required for the *SNN*-mediated inhibition of HPV16 PsV infection.

A previous study of stannin showed that it could regulate cell cycle progression [44]. Furthermore, HPV infection requires progression of the cell cycle [13]. We therefore investigated the possibility of a link between stannin and the cell cycle by examining the DNA content of cells stably overexpressing *Luciferase* or *SNN* and cultured in either complete or serum-free growth medium. When cells were incubated in complete growth medium, stained with the DNA-binding dye DAPI and analysed by flow cytometry, stannin did not affect the proportion of cells in the G1, S and G2 phases of the cell cycle nor generate a population of cells with sub-G1 DNA content, indicative of apoptosis (Fig. S4b). In addition, *SNN* overexpression did not prevent G1 growth arrest induced by incubation of cells in serum-free medium. Thus, the anti-HPV effect of stannin does not depend on stannin-mediated regulation of the cell cycle.

HPV16 infection requires furin, a cellular proprotein convertase that cleaves the N-terminus of the HPV16 L2 protein at the cell surface [5]. In the absence of furin action, HPV16 virions can enter cells and disassemble, but their escape from the endosomal compartment is impaired. To determine if *SNN* overexpression inhibited HPV16 L2 cleavage by furin, we used a recombinant HPV16 PsV tagged with the 70-residue *Propionibacterium shermanii* transcarboxylase protein domain (PSTCD) at the N-terminus of L2 (HPV16.L2-PSTCD) upstream of the furin cleavage site [45]. Cleavage of L2-PSTCD by furin at the consensus site releases the PSTCD, allowing the full-length and cleaved forms of L2 to be resolved by SDS-polyacrylamide gel electrophoresis. HeLa cells stably overexpressing *Luciferase* or *SNN* were infected with HPV16.L2-PSTCD PsV. Lysates prepared 8 h after infection were subjected to Western blotting with an antibody ($K4_{20\text{-}38}$) specific for an L2 epitope downstream of the furin cleavage site. In agreement with previous reports, the furin-cleaved form of L2 was shorter and less abundant compared to the full-length protein and was absent in infected cells pre-treated with a furin inhibitor (Fig. S4c). The quantity of cleaved L2 was similar in control and *SNN*-overexpressing cells, demonstrating that stannin did not inhibit furin-mediated cleavage of L2.

Stannin and viral DNA co-localize to the endolysosomal compartment

We next determined where stannin localized in the cell. In order to detect stannin, a FLAG epitope tag sequence was cloned in-frame into the *SNN* cDNA at either the 5′ or 3′ position of the *SNN* open reading frame. Stable expression of *5′FLAG-SNN* or *3′FLAG-SNN* in HeLa cells inhibited HPV16-GFP infection to a similar extent as untagged stannin, but had no impact on adenovirus infection (Fig. S5). HeLa cells stably overexpressing C-terminally tagged stannin were stained with a FLAG-specific antibody and visualized by confocal immunofluorescence microscopy. We observed significant co-localization between stannin and the early endosome marker EEA1, the late endosome marker Rab9, the endolysosomal marker LAMP1 and the TGN marker TGN46, but little co-localization with the mitochondrial marker COX IV or the ER marker BiP (Fig. 3a, b). HPV16 PsV infection did not affect stannin co-localization with these markers. These results indicate that stannin is broadly distributed in a variety of intracellular organelles in the retrograde transport pathway whether or not the cells were infected with HPV16 PsV.

To examine whether HPV16 trafficking involves passage through cellular compartments containing stannin, we generated HPV16 PsV incorporating plasmid DNA labelled with the nucleotide analogue 5-ethynyl-2′-deoxyuridine (EdU) [46]. Unlabelled HeLa cells stably overexpressing FLAG-tagged stannin were infected with EdU-labelled HPV16 PsV for 8 or 24 h and stained with the Click-iT EdU Imaging reaction cocktail to visualize the pseudovirus DNA and with anti-FLAG to detect stannin. Confocal immunofluorescence microscopy revealed significant overlap between pseudovirus DNA and stannin (Fig. 3c, d). Collectively, these results indicate that stannin co-localizes with HPV16 PsV DNA in a range of retrograde compartments during intracellular trafficking during entry.

Identification of stannin domains required for inhibition of HPV16 entry

Stannin is comprised of N-terminal transmembrane, linker, and C-terminal domains. We performed deletion analysis of stannin to examine the contribution of these domains to its anti-HPV function (Fig. 4a). For the stannin(1–59) mutant, we deleted amino acids 60–88 comprising the cytoplasmic C-terminal domain. The stannin(1–36) mutant contained a larger deletion (removing amino acids 37–88) spanning both the linker and the C-terminal domains. Rather than deleting the N-terminal transmembrane domain of stannin, which would most likely abolish the membrane localization of the protein, we instead replaced it with the transmembrane domain of TLR9 [stannin(TLR9TM) mutant], which targets TLR9 to the ER [47]. Each mutant was further engineered to contain a HA tag at the N-terminus to facilitate intracellular detection. The HA tag did not impair the ability of full-length stannin to inhibit HPV16 PsV infection (Fig. 4b).

Following overexpression in HeLa cells, we found that the stannin(1-59) mutant, like full-length (FL) stannin, localized to both EEA1- and LAMP1-positive compartments (Fig. 4c, d), and retained the antiviral activity of the wild-type stannin (Fig. 4b). In contrast, stannin(1-36) co-localized almost exclusively with LAMP1-positive structures and failed to inhibit HPV16-GFP PsV infection. The chimeric stannin(TLR9TM) protein was not found in endosomes, and instead formed a reticular network suggestive of the ER, as expected (Fig. 4b). This chimera also failed to inhibit HPV16 entry. Taken together, these data suggest that the C-terminal domain of

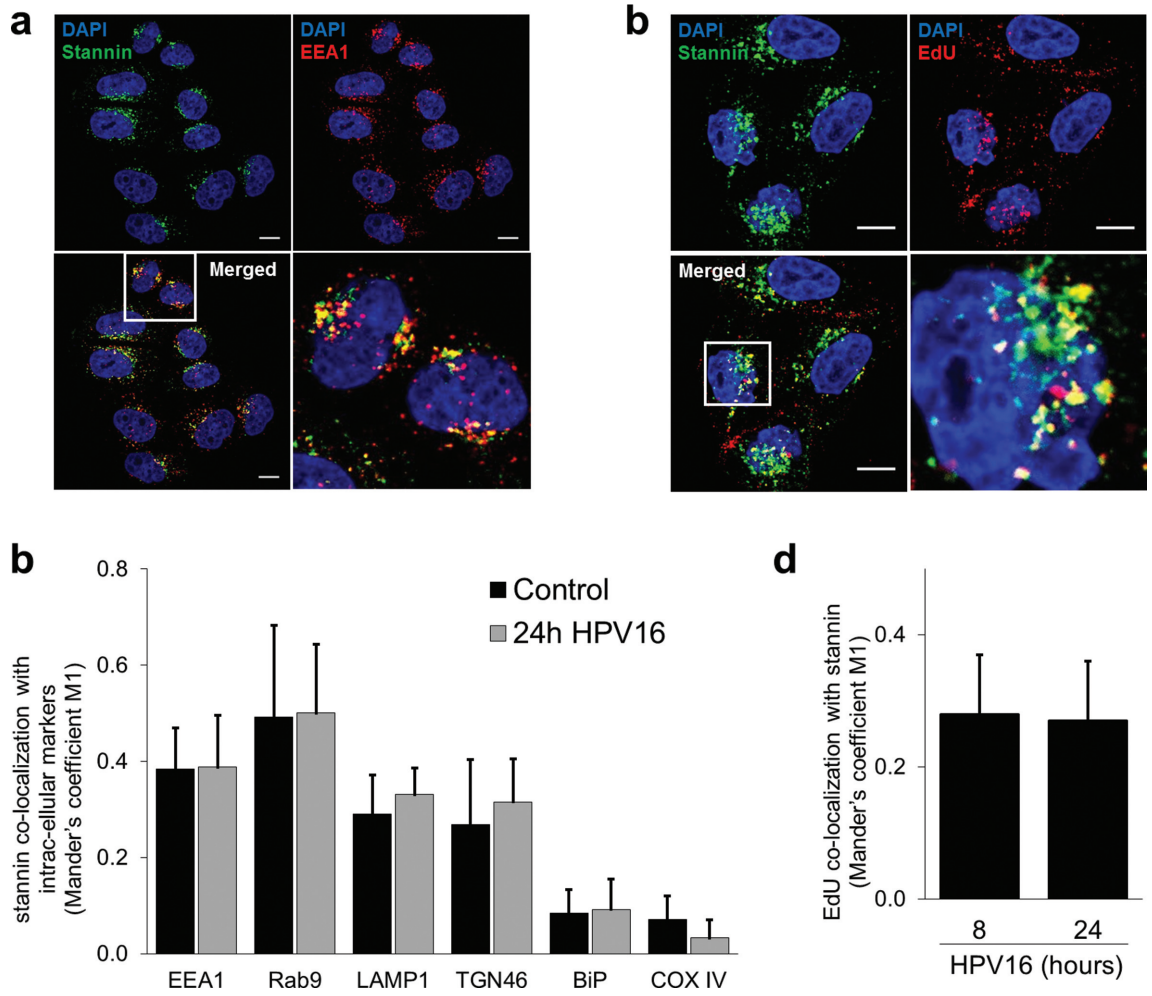

Fig. 3. Stannin co-localizes with the endolysosomal compartment and incoming HPV16 genomes. (a) HeLa cells stably overexpressing FLAG-tagged stannin were seeded onto coverslips, fixed, and immunostained with antibodies against FLAG (stannin, green) and EEA1 (red). Nuclei were stained with DAPI (blue). Co-localization of FLAG and EEA1 appears yellow in the bottom panels. The boxed area in the merged image is displayed separately at a higher magnification at the lower right. The same confocal slice is shown in each panel. Scale bar: 10 µm. (b) HeLa cells stably overexpressing FLAG-tagged stannin were seeded onto coverslips and either remained untreated (control, black bars) or incubated with HPV16 PsV (3×10^4 vge cell^{-1}, grey bars). Twenty four h later cells were fixed and immunostained with antibodies against FLAG (to detect stannin) and against EEA1, Rab9, LAMP1, TGN46, BiP or COX IV. The bar graph shows the extent of overlap between FLAG staining and that of the various subcellular markers in control and infected cells, analysed with the JACoP plugin for ImageJ. For each analysis, the mean and SD were calculated from more than 100 cells and are representative of two independent experiments. (c) HeLa cells stably overexpressing FLAG-tagged stannin were seeded onto coverslips and incubated with 5-ethynyl-2′-deoxyuridine (EdU)-labelled HPV16 PsV (3×10^4 vge cell^{-1}). After 8 h the cells were fixed, processed with the Click-iT imaging kit to stain the viral pseudogenomes (EdU, red), and then immunostained with a FLAG antibody (stannin, green). Nuclei were stained with DAPI (blue). Co-localization of FLAG and EdU appears yellow in the bottom panels. The boxed area in the merged image is displayed separately at a higher magnification at the lower right. The same confocal slice is shown in each panel. Scale bar: 10 µm. (d) HeLa cells infected and processed as described in (c) 8 or 24 h after infection. The bar graph shows the extent of co-localization between EdU and stannin staining analysed with the JACoP plugin for ImageJ. For each analysis, the mean and SD were calculated from more than 100 cells and are representative of three independent experiments. For (a) and (c), images are representative of three or more independent experiments.

stannin is required neither for stannin localization to the early endosome nor for inhibition of HPV16 infection. In contrast, deletion of both the C-terminal and the linker domains mislocalized stannin(1–36) to LAMP1-positive compartments and rendered the protein incapable of blocking viral entry. Moreover, the intact linker and C-terminus of stannin, when ectopically localized to the ER, did not inhibit HPV. Thus, the presence of the N-terminal transmembrane domain and linker domain is required for proper *SNN* localization and anti-HPV activity.

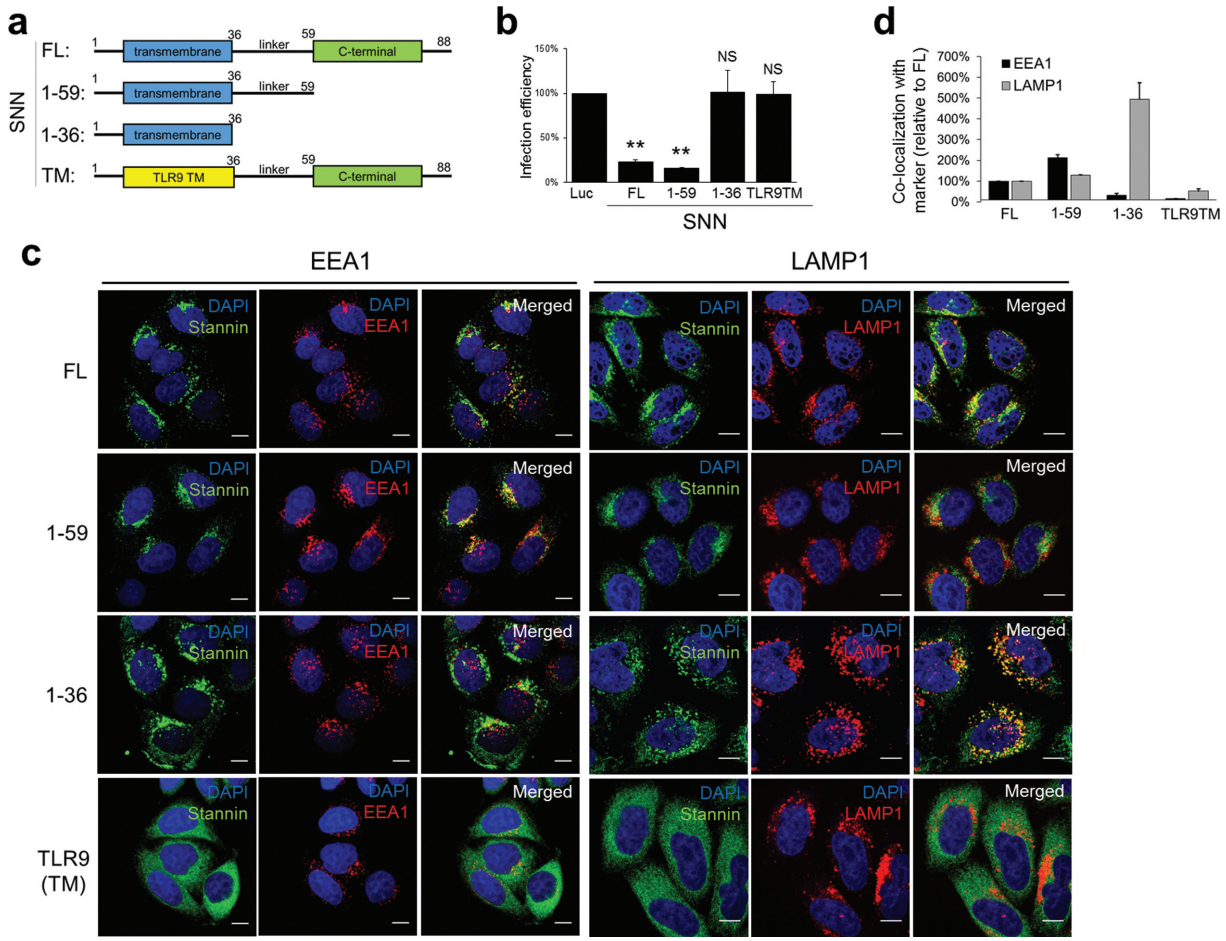

Fig. 4. Mapping domains of stannin required for antiviral activity. (a) Schematic diagrams of domain composition of full-length (FL) and mutant stannin. Stannin(1–36) and stannin(1–59) mutants comprise the first 36 and 59 amino acids of stannin, respectively. The stannin(TLR9TM) mutant is a chimera of FL stannin and 20 amino acids from the TLR9 transmembrane (TLR9TM) domain. (b–d) HeLa cells were transduced with lentiviruses encoding *Luciferase* (control), HA-tagged full-length (FL) stannin, or the different HA-tagged stannin mutants. (b) Cells transduced with the indicated gene were infected with HPV16-GFP PsV (100–200 vge cell^{-1}) for 48 h, fixed and assayed by flow cytometry for GFP expression. Infection efficiency was calculated as described in Methods. Results show the mean and SD from three independent experiments, normalized to cells lacking transduced stannin. (c) Transduced cells were seeded onto glass coverslips, fixed and immunostained with antibodies against HA (stannin, green) and EEA1 or LAMP1 (both red). Nuclei were stained with DAPI (blue). Co-localization of stannin and EEA1 appears yellow in the right column in each set. The same confocal slice is shown in each row of each set. Scale bar: 10 µm. (d) Transduced cells were processed for immunofluorescence microscopy as described in (c) and images analysed for co-localization between stannin and either EEA1 (black bars) or LAMP1 (grey bars) with the JACoP plugin for ImageJ. Results show the mean and SD from two independent experiments with at least 100 cells analysed for each co-localization, normalized to cells expressing full-length stannin. Where indicated, statistical significance was determined by an unpaired two-tailed *t*-test: $^{**}P<0.01$. NS, not significant.

Stannin overexpression inhibits HPV16 transport to the TGN

The localization of stannin in the endosomal compartment suggested that *SNN* overexpression might inhibit HPV16 entry by perturbing virus uptake into, uncoating in or escape from the endosome. To examine HPV16 attachment to the plasma membrane, HaCaT cells stably overexpressing *Luciferase* or *SNN* were incubated with HPV16 PsV at 4 °C to allow virus binding but not internalization. After 1 h, unbound virus was washed away, and cells were harvested for analysis by Western blotting with an antibody recognizing HPV16 L1. The amount of cell surface-bound L1 was similar for the two cell lines (Fig. 5a), indicating that stannin does not inhibit viral attachment to target cells.

To study virus uptake and the initiation of uncoating, HaCaT cells were incubated with HPV16 PsV for 8 h at 37 °C, trypsinized to remove cell surface-bound virions and stained with an antibody (33L1-7) that recognizes a linear epitope within L1 that is inaccessible in intact virions but exposed after internalization and uncoating [48]. 33L1-7

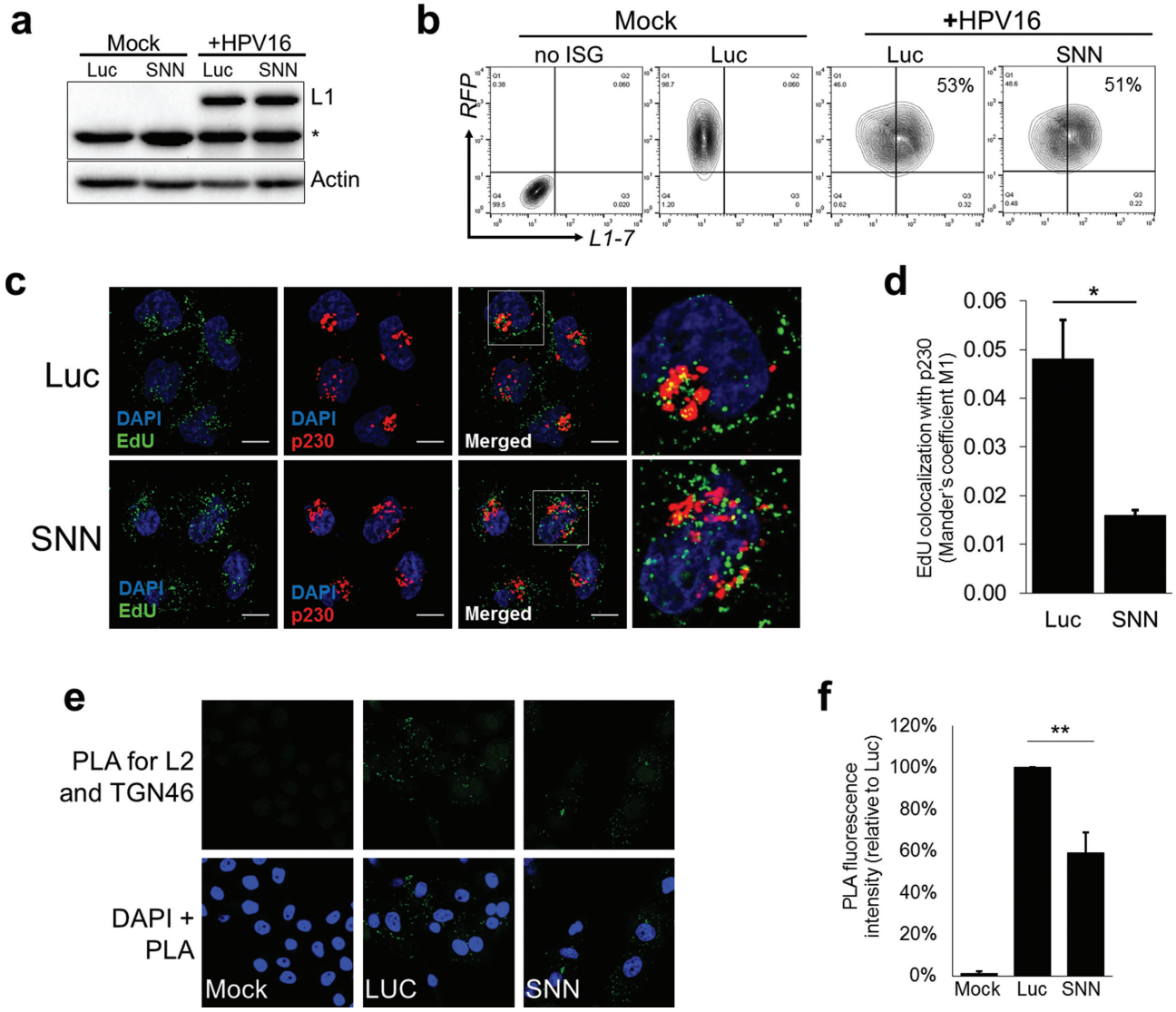

Fig. 5. Stannin overexpression does not affect virus binding or internalization but inhibits HPV16 transport to the TGN. (a) HaCaT cells stably overexpressing *Luciferase* (luc) or *SNN* were mock-infected or incubated with HPV16 PsV (1×10^4 vge cell^{-1}) for 1 h at 4 °C. Unbound virus was washed away, cells were harvested in NP40 lysis buffer and lysates were analysed by SDS-PAGE and immunoblotting with an actin or an L1 antibody. Non-specific bands are indicated with an asterisk. (b) HaCaT cells stably overexpressing *Luciferase* (control) or *SNN* were incubated with HPV16 PsV (1×10^3 vge cell^{-1}) for 8 h at 37 °C or remained untreated. Cells were trypsinized to remove surface-bound PsV, immunostained with the 33L1-7 antibody, and assayed by flow cytometry. Uninfected wild-type HaCaT cells (no ISG) were included in the experiment to serve as a TagRFP-negative gating control. The percentage of 33L1-7$^+$ cells is indicated in the upper right quadrant. (c) HeLa cells stably overexpressing *Luciferase* (Luc) or *SNN* were incubated with EdU-labelled HPV16 PsV (3×10^4 vge cell^{-1}). After 20 h the cells were fixed, processed with the Click-iT imaging kit to visualize viral pseudogenomes (EdU, green) and then immunostained with a TGN antibody (p230, red). Nuclei were stained with DAPI (blue). Co-localization of p230 and EdU appears yellow in the panels labelled merged. Boxed areas in the merged images are displayed separately in the right-most panels at a higher magnification. The same confocal slice is shown in each row. Scale bar: 10 µm. (d) HeLa cells were infected and processed as described in (c). Co-localization between EdU and p230 was analysed with the JACoP plugin for ImageJ. The mean and SD were calculated from three independent experiments with at least 100 cells counted per experiment. Statistical significance was determined by an unpaired two-tailed *t*-test: **P*<0.05. (e) HeLa cells stably overexpressing *Luciferase* were mock-infected and cells overexpressing *Luciferase* or *SNN* were infected HPV16.L2F PsV (3×10^4 vge cell^{-1}) for 16 h. Cells were processed for proximity ligation assay (PLA) with antibodies recognizing the FLAG epitope on L2 and TGN46. Nuclei were stained with DAPI (blue). Top panels show PLA signal (green); bottom panels show merged DAPI and PLA signals. Images are representative of three independent experiments. (f) HeLa cells stably overexpressing *Luciferase* or *SNN* were infected and processed as described in (e). The bar graph shows the mean and SD of the total PLA signal from three independent experiments, normalized to infected control cells. Statistical significance was determined by an unpaired two-tailed *t*-test: ***P*<0.01.

antibody binding as assessed by flow cytometry was similar in the presence and absence of overexpressed stannin (Fig. 5b), indicating that virus internalization occurs in *SNN*-overexpressing cells and that the virus initiated uncoating in these cells.

To address whether stannin might inhibit HPV16 trafficking to the TGN, we used EdU-labelled HPV16 PsV to track pseudovirus DNA within infected cells. HeLa cells stably overexpressing *Luciferase* or *SNN* were incubated with EdU-labelled HPV16 PsV, and cells were fixed and stained at various times post-infection (p.i.). We observed an approximately threefold reduction in co-localization between EdU and p230 (a TGN marker) in cells overexpressing *SNN* compared to the *Luciferase* control (Fig. 5c, d), suggesting that stannin inhibited HPV trafficking to the TGN.

We used the *in situ* proximity ligation assay (PLA) to confirm that stannin affected the arrival of L2 at the TGN. PLA is a highly sensitive method to quantitate protein co-localization that utilizes two antibodies conjugated to short oligonucleotides [49]. If the proteins of interest are within 40 nm of each other, the oligonucleotides can be ligated, the ligation product amplified and the amplified DNA labelled with fluorescent probes [50]. For this experiment, we infected control and *SNN*-overexpressing HeLa cells with HPV16 PsV containing FLAG-tagged L2 (HPV16.L2F), and after 16 h performed PLA using anti-FLAG antibody (to recognize L2) and an antibody recognizing TGN46, a marker of the TGN. We used HPV16 PsV incorporating a 3xFLAG at the C-terminus of L2 (HPV16.L2F). The 3xFLAG tag is constitutively exposed on the surface of the HPV16.L2F capsids and does not require virus uncoating for detection [10]. As shown in Fig. 5(e, f), there is an approximately twofold reduction in the PLA signal in the *SNN* cells, providing further evidence that *SNN* overexpression in the endolysosomal compartment impairs the delivery of incoming virions into the TGN.

Stannin associates with the HPV16 capsid during infection and inhibits retromer recruitment

To test whether stannin physically interacts with incoming HPV16 pseudovirions, we transduced HeLa cells with *SNN* encoding a C-terminal HA tag (*3′HA-SNN*). Cells stably overexpressing *Luciferase* or *3′HA-SNN* were infected for 8 h with HPV16.L2F PsV (containing L1 and FLAG-tagged L2) or with HPV16.L1 PsV, which contains only the L1 protein without L2. We lysed the infected cells with a high ($5\ mg\ ml^{-1}$) concentration of digitonin, a non-ionic detergent which efficiently solubilizes membrane protein complexes [51]. Lysates were immunoprecipitated with a HA antibody and assayed by Western blotting with antibodies recognizing L1 and the FLAG tag (to detect L2). No immunoprecipitation of L1 or L2 occurred from cells lacking HA-*SNN* expression. In contrast, both L1 and L2 reproducibly co-precipitated with stannin early after infection with HPV16.L2F (Fig. 6a), demonstrating complex formation between the PsV particle and stannin. We also observed co-immunoprecipitation between stannin and L1 and L2 in extracts prepared in buffers containing the non-ionic detergent Nonidet-P40 and the chemical crosslinker dithiobis (succinimidyl propionate) (data not shown). Notably, L1 was also precipitated, albeit at a lower level, from cells infected with PsV containing only L1 (Fig. 6a), showing that L1 was sufficient for stannin binding. We conclude that L2 as well as L1 is co-immunoprecipitated with PsV particles containing both viral proteins because they are tightly associated in the complete PsV particle. These results indicate that stannin stably associates with the incoming viral particle via an interaction with L1, although we have not ruled out the possibility that the interaction between L1 and stannin is indirect. The reduced association observed with the L1-only particles suggested that L2 modulates this interaction.

Retromer is a protein complex that binds directly to the L2 protein and plays a key role in HPV16 escape from the endosome to the Golgi [8, 22]. We hypothesized that decreased trafficking of HPV16 to the TGN in cells stably overexpressing *SNN* might be associated with decreased recruitment of L2 to the retromer. We used PLA to assess if L2 is in close proximity to the retromer subunit VPS35 following infection with HPV16.L2F [22]. Notably, *SNN* overexpression led to an approximately fourfold decrease in the PLA signal between L2 and VPS35 (Fig. 6b, c). The dramatic reduction in signal indicates that stannin overexpression inhibited the interaction between L2 and the retromer.

Stannin overexpression does not disrupt endolysosomal morphology or retrograde transport of other cargo proteins

Stannin overexpression could block HPV trafficking by changing endolysosomal maturation or retrograde transport in general. First, we examined the morphology and intracellular distribution of endolysosomes in *SNN*-overexpressing cells. Fig. S6(a) shows that the morphology and subcellular localization of EEA1- and LAMP1-positive compartments was not noticeably altered by *SNN* overexpression in HeLa cells. Moreover, *SNN* overexpression did not change the extent of co-localization between EEA1 and LAMP1 (Fig. S6b). Similarly, *SNN* overexpression had no noticeable effect on the size, morphology or intracellular distribution of the Golgi apparatus or TGN, as assessed by staining for the markers GM130 and p230 (Fig. 7a, b).

Further, we examined intracellular transport of two well-established model cargo proteins that reach the TGN through the retrograde pathway, the cholera toxin B subunit (CTXB) [52] and cation-independent mannose phosphate receptor (CIMPR) [53]. Stannin overexpression had no impact on the co-localization of these cargo proteins and TGN markers (Fig. 7). Taken together, these results indicate that stannin overexpression does not perturb cellular endosomal trafficking pathways of these two retromer cargoes tested.

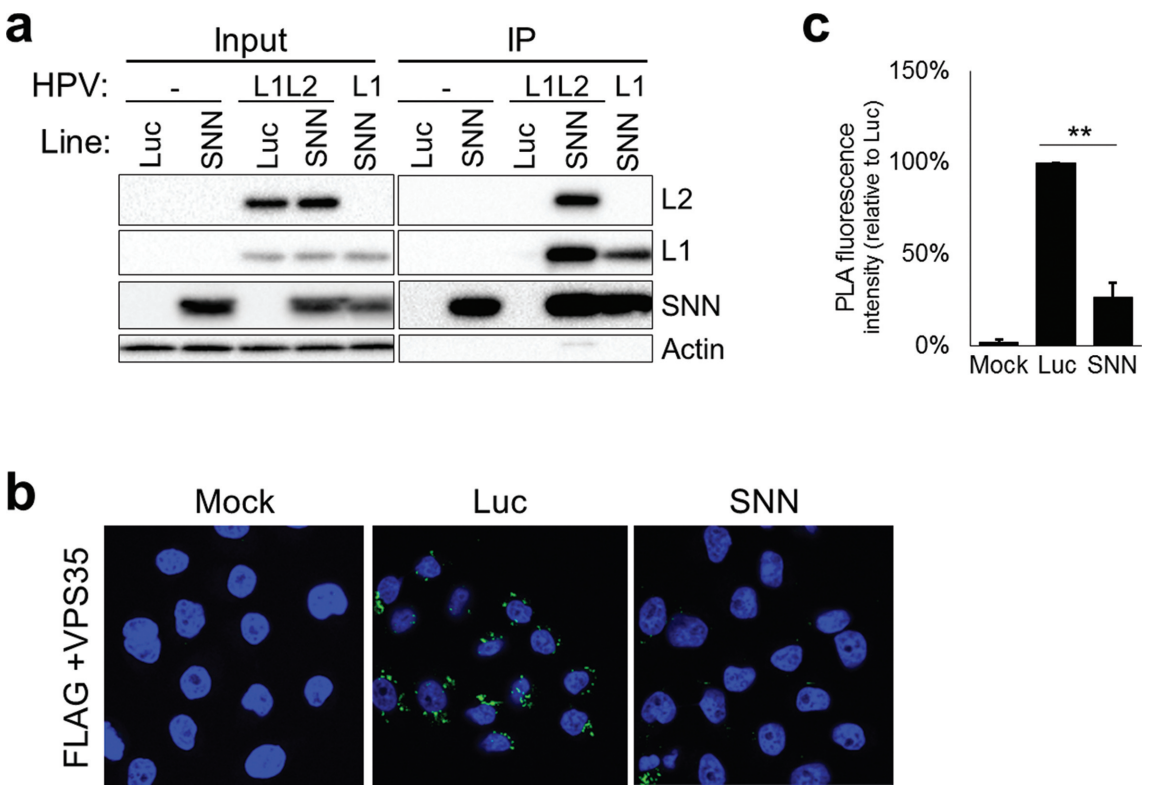

Fig. 6. HPV16 associates with stannin. (a) HeLa cells stably overexpressing *Luciferase* or HA-tagged stannin were mock-infected or infected with HPV16.L2F (L1L2) or with HPV16 L1-only (L1) PsV (1×10^4 vge cell^{-1}). Eight hours later, cells were trypsinized to remove surface-bound virions and lysed in buffer containing 0.5 % digitonin. Lysates were precipitated with a HA antibody-bead conjugate, and immunoprecipitates were analysed by SDS-PAGE and Western blotting with antibodies specific for actin, HA (stannin), HPV16 L1 and FLAG (to visualize L2). Input lanes show 5 % of each lysate prior to immunoprecipitation (IP). For each of the indicated antibodies, images for the input and IP sets of samples were derived from the same blot. (b) HeLa cells stably overexpressing *Luciferase* or *SNN* were mock-infected or infected with HPV16.L2F (6×10^3 vge cell^{-1}). Eight hours later, cells were fixed, reacted with antibodies against FLAG (L2) and VPS35 (retromer) and processed for the proximity ligation assay (green). Nuclei were stained with DAPI (blue). A single confocal slice is shown in each panel. Images are representative of three or more independent experiments. (c) HeLa cells stably overexpressing *Luciferase* or *SNN* were infected and processed as described in (b). The bar graph shows the mean and SD of the total PLA signal from three independent experiments, normalized to infected control cells. Statistical significance was determined by an unpaired two-tailed *t*-test: $^{**}P<0.01$.

Stannin promotes HPV16 L1 and L2 degradation

HPV that cannot escape the endosomal compartment may ultimately be sorted to the lysosome where it is degraded [23]. We therefore reasoned that a block in endosome-to-TGN viral trafficking imposed by *SNN* overexpression might lead to increased degradation of incoming HPV16. To test this, we infected control and *SNN*-overexpressing HeLa cells with HPV16 PsV at 37 °C for 16 or 24 h. Cells were then trypsinized to remove cell surface-bound virions, and cell lysates were analysed by Western blotting for L1 and L2. At 16 and 24 h p.i., *SNN* overexpression led to an increase in the intensity of a low molecular weight band corresponding to an L1 cleavage product (Fig. 8a, b). The appearance of this L1 cleavage product was abolished by treatment of infected cells with chloroquine, an inhibitor of lysosome acidification (Fig. S7). *SNN* overexpression also led to an approximately twofold decrease in the levels of full-length L1 and L2 proteins at 16 and 24 h p.i. (Figs 8a, b and S7). To determine whether the observed reduction in L1 and L2 protein levels was accompanied by degradation of pseudovirus reporter plasmid DNA, we measured the quantity of plasmid DNA in infected cells 24 h p.i. Total DNA was extracted from infected cells and assayed by qPCR with primers specific for both the cellular and pseudoviral genomes. *SNN* overexpression led to an approximately twofold reduction in the number of HPV16 pseudogenomes over a range of virus doses (Fig. 8c).

The increased abundance of a chloroquine-sensitive L1 cleavage product in *SNN*-overexpressing cells, together with the reduced amounts of pseudovirus DNA and full-length L1 and L2 in these cells at late times after infection, suggested that incoming virus was directed to the lysosome for degradation. To test this hypothesis, we used PLA to determine whether there were increased levels of HPV16

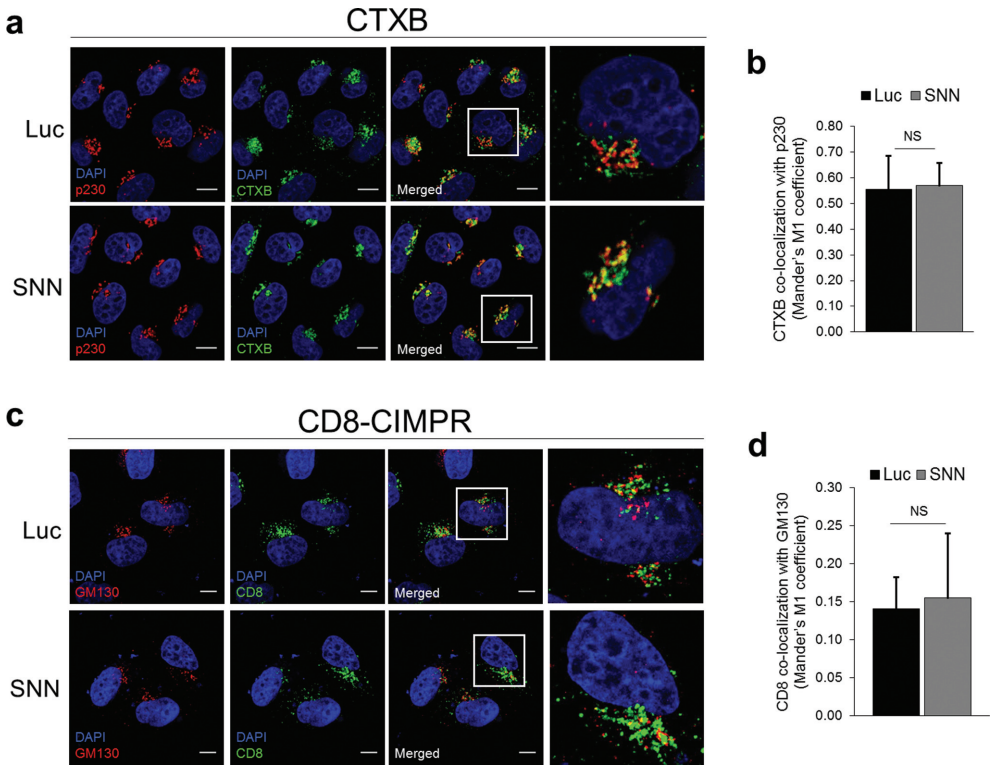

Fig. 7. SNN overexpression does not inhibit Golgi trafficking of cholera toxin and CD8-CIMPR. (a) HeLa cells stably overexpressing *Luciferase* (Luc) or *SNN* were seeded onto coverslips and incubated for 1 h with AF488-conjugated cholera toxin B subunit (CTXB, green). Cells were then fixed and immunostained with a p230 antibody (red). Nuclei were stained with DAPI (blue). Co-localization of CTXB and p230 appears yellow in the panels labelled merged. The boxed area in the merged image is displayed separately at a higher magnification in the far-right panels. The same confocal slice is shown in each row. Scale bar: 10 µm. Images are representative of three independent experiments. (b) Co-localization analysis of CTXB and p230 staining calculated with the JACoP plugin for ImageJ. The mean and SD were calculated from more than 100 cells and are representative of three independent experiments. The differences were not statistically significant (NS) as determined by an unpaired two-tailed *t*-test. (c) HeLa cells stably overexpressing *Luciferase* (Luc) or *SNN* were seeded onto coverslips and transfected with a vector encoding the CD8-CIMPR chimeric protein. Forty eight hours later, the cells were incubated for 3 h with anti-CD8 antibody (green) at 37 °C, fixed and immunostained with a GM130 antibody (red). Nuclei were stained with DAPI (blue). Co-localization of CD8 and GM130 appears yellow in panels labelled merged. The boxed area in the merged image is displayed separately at a higher magnification in the far-right panels. The same confocal slice is shown in each panel. Scale bar: 10 µm. Images are representative of three independent experiments. (d) Co-localization analysis of CD8 and GM130 staining calculated with the JACoP plugin for ImageJ. The mean and SD were calculated from more than 100 cells and are representative of three independent experiments. The differences were not statistically significant (NS) as determined by an unpaired two-tailed *t*-test.

pseudovirions in LAMP1-positive subcellular compartments in *SNN*-overexpressing cells. *SNN* overexpression led to an almost twofold increase in the PLA signal between the FLAG-tagged L2 protein and the lysosome marker LAMP1 late after infection (Fig. 8d, e). Taken together, these data indicate that *SNN* overexpression causes incoming HPV to be degraded in the lysosome.

DISCUSSION

Here we report an ISG overexpression screen to identify genes that regulate HPV16 entry into human epithelial cells. ISG overexpression studies for other viruses typically identified common sets of ISGs with broad antiviral activity, such as *IRF1* and *MyD88*, which encode transcription factors that activate IFN-stimulated response element-mediated gene expression and TLR signalling, and *cGAS*, which encodes a cytosolic DNA sensor involved in antiviral resistance [54]. However, overexpression of *IRF1, MyD88* and *cGAS* did not inhibit HPV infection in our screen, suggesting that HPV16 may use a unique strategy to evade intracellular immune surveillance. Rather, we identified a unique set of genes, including *SNN*, *thrombomodulin* (THBD) and *vacuole membrane protein 1* (VMP1), which are not widely known for antiviral activity. Several of the top hits conferred protection against several HPV types (but not other viruses) and were active in both HeLa and HaCaT cells. Some of these hits participate in cellular processes known to play a role in HPV16 entry. For example, heparanase is an enzyme

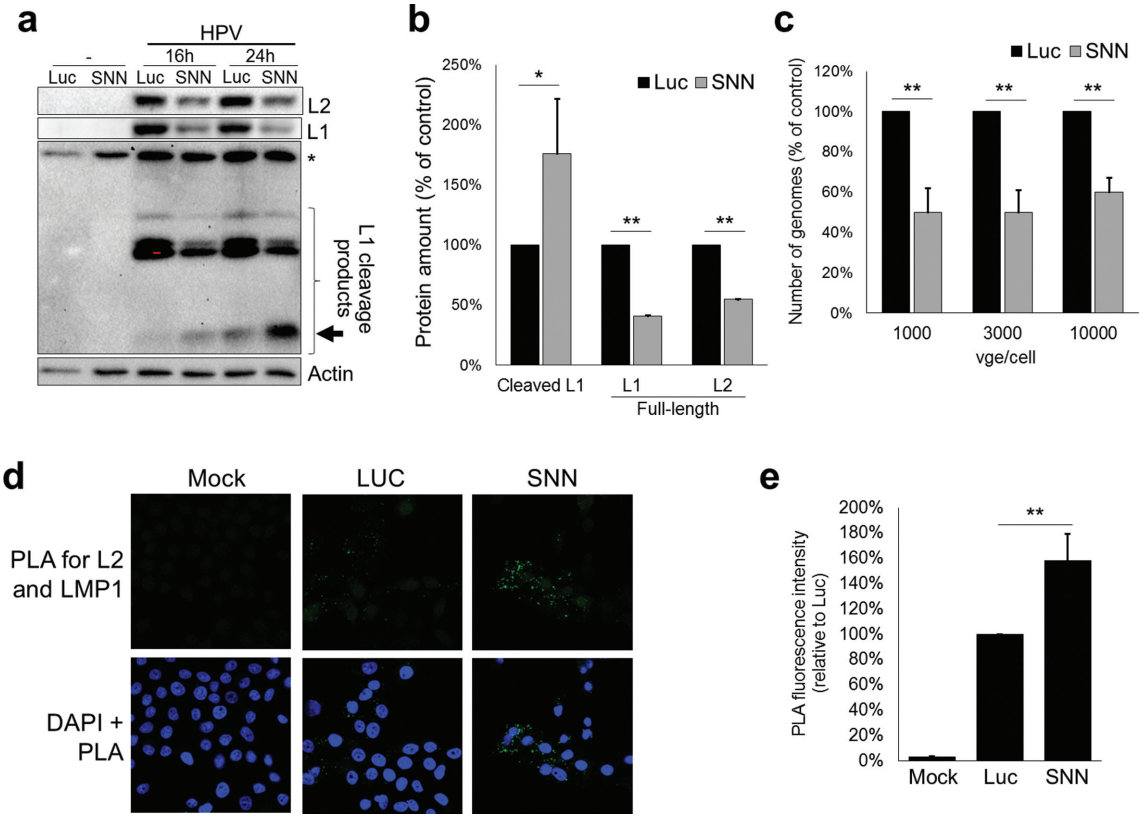

Fig. 8. Stannin promotes HPV16 capsid protein and genome degradation. (a) HeLa cells stably overexpressing *Luciferase* or untagged stannin were mock-infected or infected with HPV16.L2F PsV (1×10^4 vge cell^{-1}) for 16 or 24 h. Cells were trypsinized to remove surface-bound virions, lysed and analysed by Western blotting with antibodies against actin, L1 and FLAG (L2). Non-specific bands are indicated with an asterisk. Full-length L2 and L1 are shown in the top two panels. The major small L1 cleavage product is shown with an arrow. (b) Quantitation of chemiluminescence signal intensities from the blot shown in (a) corresponding to samples prepared from cells infected for 24 h. 'Cleaved L1' corresponds to the smallest cleavage fragment of L1 indicated with an arrow in (a). Results show the mean and SD from three (cleaved L1) or two (full-length L1 and L2) independent experiments. Statistical significance was determined by an unpaired two-tailed *t*-test: $^{**}P\leq0.01$, *, $P\leq0.05$. (c) HeLa cells stably overexpressing *Luciferase* or *SNN* were infected with 1×10^3, 3×10^3 or 1×10^4 vge cell^{-1} of HPV16 PsV as indicated. Twenty four h later, the cells were trypsinized to remove surface-bound virions. Extracted DNA was assayed by qPCR for *neomycin* gene copy number (pseudoviral genomes) and values were normalized to *GAPDH* gene copy number (cellular DNA). Results show the mean and SD from three independent experiments. Statistical significance was determined by an unpaired two-tailed *t*-test: $^{**}P\leq0.01$. (d) HeLa cells stably overexpressing *Luciferase* or *SNN* were mock-infected or infected with HPV16.L2F (6×10^3 vge cell^{-1}). Eight hours later, all cells were fixed, reacted with antibodies against FLAG (L2) and LAMP1, and processed for the proximity ligation assay (green). Nuclei were stained with DAPI (blue). A single confocal slice is shown in each panel. Top panels show PLA signal (green); bottom panels show merged DAPI and PLA signals. Images are representative of three or more independent experiments. (e) HeLa cells stably overexpressing *Luciferase* or *SNN* were infected and processed as described in (d). The bar graph shows the mean and SD of the total PLA signal from three independent experiments, normalized to infected control cells. Statistical significance was determined by an unpaired two-tailed *t*-test: $^{**}P<0.01$.

that cleaves HSPGs, which are critical for HPV16 binding to the cell surface [3], and VMP1 was reported to initiate autophagy, an antiviral mechanism that limits HPV16 infection [41, 55].

The atypical ISG signature revealed by our screen may reflect the retrograde cell entry pathway utilized by HPVs to traffic to the nucleus [56]. Consistent with this idea, the screen hit ankyrin repeat and FYVE domain containing 1 regulates the subcellular localization of the retromer complex [57], a key factor for HPV16 trafficking to the TGN. Other hits, such as stannin, were not previously known to affect processes involved in HPV infection. Because the retrograde pathway comprises a number of membrane-bound organelles, including the endosome, the Golgi and the ER, use of this entry pathway by HPV may sequester the virus away from the typical antiviral effector ISG products found in the cytosol.

Here we focused on the role of stannin in inhibiting HPV16 cell entry. *SNN* is an evolutionary conserved gene with poorly understood biological function. We show that

overexpression of *SNN* inhibits HPV infection, and knockout of *SNN* enhances HPV16 infection. Overexpressed stannin inhibited infection by HPV16 and HPV18, which are responsible for ~70 % of cervical cancer and the vast majority of other HPV-associated mucosal cancer, as well as by HPV5, which infects skin cells. The N-terminal transmembrane domain and the linker region of stannin, but not the cytoplasmic C-terminal helix are required for its proper localization and HPV inhibitory activity. Although stannin was present in the ISG library, it is not induced by IFNs in HaCaT cells and is therefore not an ISG in this system. Our experiments also revealed that *SNN* is constitutively expressed in human epithelial cells including keratinocytes. As shown by analysis of *SNN*-knockout cells constructed by CRISPR-mediated mutagenesis, basal levels of the stannin protein are sufficient to inhibit infection of HeLa cells by HPV16 PsV. In this regard, stannin is similar to the restriction factor APOBEC3A whose endogenous levels significantly impair HPV16 cell entry even in the absence of IFN treatment [32].

Our results showed that stannin co-localized with internalized HPV16 PsV genomes in retrograde compartments, suggesting that stannin might directly interact with HPV virions. Indeed, co-immunoprecipitation studies showed that stannin binds to the capsid. This binding is mediated by L1, since L1-only PsV bind stannin, but binding may be indirect and appears to be modulated by L2.

We performed a series of experiments to determine the step in HPV16 infection regulated by stannin. *SNN* overexpression did not affect attachment, uptake or uncoating of HPV16 PsV in infected cells. In contrast, *SNN* overexpression decreased the abundance of HPV16 PsV in the TGN, suggesting that stannin disrupts proper HPV trafficking. Indeed, *SNN* overexpression disrupted the retromer-L2 interaction, as shown by the reduced PLA signal between L2 and the retromer subunit VPS35. However, further analysis revealed that the levels of full-length viral proteins and viral DNA are reduced by 16 h p.i. in *SNN*-overexpressing cells, complicating the interpretation of the reduced co-localization of viral DNA and L2 protein in the TGN at late times of infection.

The increased degradation of viral capsid proteins and pseudovirus DNA appeared to be mediated by lysosomal degradation because appearance of the major L1 cleavage product required acidification of the lysosome and increased levels of L2 were detected in LAMP1-positive compartments. Based on these results, we propose that endocytosed HPV virions enter the endosome and L1 interacts with endogenously expressed stannin (Fig. S8). This interaction directly or indirectly prevents the virus from engaging the retromer. In the direct model, the inability of the retromer to engage L2 blocks HPV trafficking to the TGN, and the virus is instead routed to the lysosome where degradation occurs. Alternatively, binding of stannin to L1 may directly target the virion to the lysosome, in which case is it no longer available to engage the retromer. The association of L1 with L2 and the viral genome throughout HPV entry suggests that L1 and perhaps L1/stannin binding plays a role in endosome escape [58]. Although the mechanism by which stannin promotes degradation of HPV and affects retromer association is unknown, this process resembles a recently described pathway of lysosome targeting of HPV by α-Defensin HD5 [59].

Our study reveals that stannin can bind to incoming HPV16 capsids and act as a selective inhibitor of entry by several HPV types. Although endogenous levels of stannin inhibit HPV16 infection, its role during natural infection is unclear. Stannin expression is not induced by IFN in skin keratinocytes, *SNN* knockout causes no more than a twofold increase of infection in HeLa cells, and most of our studies were performed in cells overexpressing stannin. It is possible that in some physiological conditions, stannin is an important regulator of HPV entry. For example, stannin expression may contribute to the low level of infectivity of HPV in cultured human primary keratinocytes [60]. Alternatively, the binding of L1 to stannin raises the possibility that this interaction may also affect other aspects of the virus life cycle.

METHODS

Additional detailed Methods are shown in Supplementary Material.

Cells

HeLa cells and Vero cells were purchased from the American Type Culture Collection (ATCC, #CRM-CCL-2 and #CCL-81, respectively). HeLa-sen2 cells, a clone of HeLa cells, were reported previously [61]. *ATG5−/−* HeLa cells were produced by CRISPR Cas9-mediated mutation of the *ATG5* gene. 293TT and HaCaT cells were obtained from Christopher Buck (NIH) and G. Paolo Dotto (Massachusetts General Hospital), respectively. Primary neonatal human foreskin keratinocytes were purchased from Lonza (#192906). Primary oral mucosal keratinocytes were a generous gift of Natalia Isaeva (Yale University). All primary keratinocytes were cultured in keratinocyte serum-free basal medium supplemented with bovine pituitary extract and human recombinant epidermal growth factor from Thermo Fisher Scientific (Rockford, IL). All other cell lines were cultured in Dulbecco's modified Eagle's medium supplemented with 10 % FBS.

Viruses

HPV type 5, 16 and 18 PsV were produced as described previously by transfection of 293TT cells with plasmids encoding the viral capsid proteins and a reporter plasmid [21]. EdU-labelled HPV16 PsV were generated by incubation of transfected 293TT cells with 30 μM EdU 8 h post-transfection. All PsV were purified through Optiprep density gradient medium by ultracentrifugation. Purified PsV stocks were titred by proteinase K digestion and qPCR to determine the number of viral genome equivalents (vge). Replication-deficient recombinant human

adenovirus type 5 (Ad-GFP, #1060) and adeno-associated virus type 2 (AAV-GFP, #7004) were purchased from Vector Biolabs (Malvern, PA). JC polyomavirus PsV was generated in 293TT cells and HSV1 encoding GFP was produced in Vero cells, as previously described [62].

ISG screening and confirmation assays

Lentiviral ISG-expressing libraries were generated as previously described [30]. For the screen, HeLa cells were seeded into 96-well plates at a density of 6000 cells per well and transduced with lentiviral pseudoparticles by spinoculation at 800 ***g*** for 45 min at 37 °C in cell culture medium containing 3 % FBS, 20 mM Hepes and 4 μg ml^{-1} polybrene. Cells were infected 48 h post-transduction with HPV16-GFP PsV and harvested 48 h p.i. using the Accumax cell dissociation medium (Sigma). Cells were fixed in 1 % paraformaldehyde (PFA) and stored in PBS containing 3 % FBS until analysis by flow cytometry. Samples were analysed on a S1000 flow cytometer (Stratedigm) and analysed in FlowJo Cell Analysis software (TreeStar). To calculate the Z score, we first determined HPV16 infectivity for each ISG as a percentage of GFP-positive cells in the RFP-positive population. Z score was then computed with the STANDARDIZE function in Microsoft Excel according to the formula $Z=(X-\mu)/\sigma$ where X is infectivity, μ is the mean infectivity for all ISGs and σ is SD of the mean infectivity μ. Z scores for both screen replicates are plotted on a linear scale in Fig. 1b.

Immunofluorescence (IF) microscopy

We used HeLa and HeLa-sen2 cells for all IF experiments since they require 10 times less virus than HaCaT cells for efficient infection and because they provide better resolution of intracellular structures and virions. 2×10^4 cells were seeded onto glass coverslips (#12-545-80 from Fisher Scientific) at low density (10–20 % confluency), incubated overnight and the coverslips transferred to a fresh well on the next day. Cells were fixed at room temperature in 2 % paraformaldehyde (PFA) in PBS for 30 min. Fixed cells were simultaneously permeabilized and blocked for 30 min at room temperature in PBS containing 3 % bovine serum albumin (BSA) and 0.5 % Triton X-100. Primary and secondary antibody incubations were carried out sequentially for 1 h at room temperature in PBS containing 3 % BSA. Edu-labelled HPV16 PsV genomes were detected with the Click-iT EdU Alexa Fluor 488 Imaging Kit (#C10337) and coverslips were mounted using Prolong Diamond Antifade medium with DAPI (#P36962) from Thermo Fisher Scientific (Rockford, IL). Images were visualized with a Leica SP8 confocal microscope and processed with the ImageJ program (NIH). More than 100 cells from at least five images were counted per experiment. The extent of co-localization was measured with the JaCoP plugin of ImageJ using Mander's coefficient M1. Thresholds were set manually and kept constant for each set of images.

Immunoblotting

Cells were harvested in NP40 lysis buffer (1 % NP40 and 5 % glycerol in PBS) supplemented with a protease inhibitor cocktail and incubated for 30 min on a rotator at 4 °C. Lysates were then centrifuged at 15 000 r.p.m. for 10 min to sediment nuclei and cellular debris. Supernatants were transferred to new tubes, mixed with Laemmli buffer containing 5 % beta mercaptoethanol and boiled for 10 min at 95 °C. Proteins in each sample were separated by SDS-PAGE, transferred to a 0.2 μm PVDF membrane and incubated for 30 min in blocking buffer (Tris-buffered saline with 0.05 % Tween 20 and 5 % nonfat milk). Blots were incubated with primary antibodies diluted in blocking buffer for at least 12 h at 4 °C and then with secondary antibodies in blocking buffer for 1 h at 4 °C. Proteins were visualized by incubating the blots with the SuperSignal West Pico or West Femto chemiluminescent substrates from Thermo Fisher Scientific (Rockford, IL) and signals captured with the ChemiDoc XRS+System equipped with the Image Lab image acquisition and analysis software from Bio-Rad.

Immunoprecipitation to detect complex formation between stannin and HPV16

2×10^5 HeLa cells expressing Luciferase or HA-stannin were seeded into 60 mm dishes and incubated overnight. On the next day, some of the cells were infected with 1×10^4 vge cell^{-1} of HPV16.L2F while control cells remained uninfected. Eight hours later, cells were harvested in 0.5 ml of ice-cold digitonin lysis buffer (0.5 % digitonin, 5 % glycerol, protease inhibitor cocktail, in PBS). Lysis was allowed to proceed for 1 h on ice with shaking once every 10–15 min to promote protein extraction. Insoluble cellular material was removed by centrifugation at maximum speed for 10 min in a tabletop centrifuge (Eppendorf). Supernatants were incubated with 10 μL of magnetic anti-HA beads overnight at 4 °C on a rotator. Beads were washed twice in PBS, bound proteins eluted in 2x Laemmli buffer and eluates analysed by SDS-PAGE and Western blotting.

Funding information
A. L. was supported by a National Institutes of Health (NIH) postdoctoral training grant T32 AI007019 and an individual Ruth L. Kirschstein National Research Service Award F32 AI118315; A. E. was supported in part by the Yale Gruber Science Fellowship; W. Z. was supported by an individual Ruth L. Kirschstein National Research Service Award F32 AI114132. M. C. was supported by NIH predoctoral training grant T32 AI055403. This study was supported by funding from the Howard Hughes Medical Institute and NIH R01 grant AI054359 (to A. I.); and NIH P01 grant CA016038 and R01 grant AI102876 (to D. D.).

Acknowledgements
We thank Drs Chris Buck, Pat Day, Martin Sapp, Samuel Campos, Martin Muller, Matthew Seaman and Charles Rice for essential reagents, Saige Pompura for technical assistance, Eric Song for preparing Fig. S8 and Jan Zulkeski for editorial assistance.

Conflicts of interest
The authors declare that there are no conflicts of interest.

References
1. Parkin DM. The global health burden of infection-associated cancers in the year 2002. *Int J Cancer* 2006;118:3030–3044.
2. Psyrri A, DiMaio D. Human papillomavirus in cervical and head-and-neck cancer. *Nat Clin Pract Oncol* 2008;5:24–31.

3. Richards KF, Bienkowska-Haba M, Dasgupta J, Chen XS, Sapp M. Multiple heparan sulfate binding site engagements are required for the infectious entry of human papillomavirus type 16. *J Virol* 2013;87:11426–11437.
4. Cerqueira C, Samperio Ventayol P, Vogeley C, Schelhaas M. Kallikrein-8 proteolytically processes human papillomaviruses in the extracellular space to facilitate entry into host cells. *J Virol* 2015; 89:7038–7052.
5. Richards RM, Lowy DR, Schiller JT, Day PM. Cleavage of the papillomavirus minor capsid protein, L2, at a furin consensus site is necessary for infection. *Proc Natl Acad Sci USA* 2006;103:1522–1527.
6. Raff AB, Woodham AW, Raff LM, Skeate JG, Yan L *et al.* The evolving field of human papillomavirus receptor research: a review of binding and entry. *J Virol* 2013;87:6062–6072.
7. Schelhaas M, Shah B, Holzer M, Blattmann P, Kühling L *et al.* Entry of human papillomavirus type 16 by actin-dependent, clathrin- and lipid raft-independent endocytosis. *PLoS Pathog* 2012;8: e1002657.
8. Lipovsky A, Popa A, Pimienta G, Wyler M, Bhan A *et al.* Genome-wide siRNA screen identifies the retromer as a cellular entry factor for human papillomavirus. *Proc Natl Acad Sci USA* 2013;110: 7452–7457.
9. Day PM, Thompson CD, Schowalter RM, Lowy DR, Schiller JT. Identification of a role for the trans-Golgi network in human papillomavirus 16 pseudovirus infection. *J Virol* 2013;87:3862–3870.
10. Zhang W, Kazakov T, Popa A, DiMaio D. Vesicular trafficking of incoming human papillomavirus 16 to the Golgi apparatus and endoplasmic reticulum requires γ-secretase activity. *MBio* 2014;5: e01777-14–01714.
11. Laniosz V, Dabydeen SA, Havens MA, Meneses PI. Human papillomavirus type 16 infection of human keratinocytes requires clathrin and caveolin-1 and is brefeldin a sensitive. *J Virol* 2009;83: 8221–8232.
12. Gräßel L, Fast LA, Scheffer KD, Boukhallouk F, Spoden GA *et al.* The CD63-syntenin-1 complex controls post-endocytic trafficking of oncogenic human papillomaviruses. *Sci Rep* 2016;6:32337.
13. Pyeon D, Pearce SM, Lank SM, Ahlquist P, Lambert PF. Establishment of human papillomavirus infection requires cell cycle progression. *PLoS Pathog* 2009;5:e1000318.
14. Aydin I, Weber S, Snijder B, Samperio Ventayol P, Kühbacher A *et al.* Large scale RNAi reveals the requirement of nuclear envelope breakdown for nuclear import of human papillomaviruses. *PLoS Pathog* 2014;10:e1004162.
15. Aydin I, Villalonga-Planells R, Greune L, Bronnimann MP, Calton CM *et al.* A central region in the minor capsid protein of papillomaviruses facilitates viral genome tethering and membrane penetration for mitotic nuclear entry. *PLoS Pathog* 2017;13:e1006308.
16. Calton CM, Bronnimann MP, Manson AR, Li S, Chapman JA *et al.* Translocation of the papillomavirus L2/vDNA complex across the limiting membrane requires the onset of mitosis. *PLoS Pathog* 2017;13:e1006200.
17. DiGiuseppe S, Luszczek W, Keiffer TR, Bienkowska-Haba M, Guion LG *et al.* Incoming human papillomavirus type 16 genome resides in a vesicular compartment throughout mitosis. *Proc Natl Acad Sci USA* 2016;113:6289–6294.
18. Broniarczyk J, Massimi P, Bergant M, Banks L. Human papillomavirus infectious entry and trafficking is a rapid process. *J Virol* 2015;89:8727–8732.
19. Kajitani N, Satsuka A, Kawate A, Sakai H. Productive lifecycle of human papillomaviruses that depends upon squamous epithelial differentiation. *Front Microbiol* 2012;3:152.
20. DiGiuseppe S, Bienkowska-Haba M, Guion LG, Sapp M. Cruising the cellular highways: How human papillomavirus travels from the surface to the nucleus. *Virus Res* 2017;231:1–9.
21. Buck CB, Pastrana DV, Lowy DR, Schiller JT. Generation of HPV pseudovirions using transfection and their use in neutralization assays. *Methods Mol Med* 2005;119:445–462.
22. Popa A, Zhang W, Harrison MS, Goodner K, Kazakov T *et al.* Direct binding of retromer to human papillomavirus type 16 minor capsid protein L2 mediates endosome exit during viral infection. *PLoS Pathog* 2015;11:e1004699.
23. Bergant Marušič M, Ozbun MA, Campos SK, Myers MP, Banks L. Human papillomavirus L2 facilitates viral escape from late endosomes via sorting nexin 17. *Traffic* 2012;13:455–467.
24. Wang JW, Roden RB. L2, the minor capsid protein of papillomavirus. *Virology* 2013;445:175–186.
25. Pim D, Broniarczyk J, Bergant M, Playford MP, Banks L. A Novel PDZ domain interaction mediates the binding between human papillomavirus 16 L2 and sorting nexin 27 and modulates virion trafficking. *J Virol* 2015;89:10145–10155.
26. Burd C, Cullen PJ. Retromer: a master conductor of endosome sorting. *Cold Spring Harb Perspect Biol* 2014;6:pii: a016774.
27. Bronnimann MP, Chapman JA, Park CK, Campos SK. A transmembrane domain and GxxxG motifs within L2 are essential for papillomavirus infection. *J Virol* 2013;87:464–473.
28. DiGiuseppe S, Keiffer TR, Bienkowska-Haba M, Luszczek W, Guion LG *et al.* Topography of the human papillomavirus minor capsid protein L2 during vesicular trafficking of infectious entry. *J Virol* 2015;89:10442–10452.
29. Kämper N, Day PM, Nowak T, Selinka HC, Florin L *et al.* A membrane-destabilizing peptide in capsid protein L2 is required for egress of papillomavirus genomes from endosomes. *J Virol* 2006; 80:759–768.
30. Schoggins JW, Rice CM. Interferon-stimulated genes and their antiviral effector functions. *Curr Opin Virol* 2011;1:519–525.
31. Schneider WM, Chevillotte MD, Rice CM. Interferon-stimulated genes: a complex web of host defenses. *Annu Rev Immunol* 2014; 32:513–545.
32. Warren CJ, Xu T, Guo K, Griffin LM, Westrich JA *et al.* APOBEC3A functions as a restriction factor of human papillomavirus. *J Virol* 2015;89:688–702.
33. Day PM, Thompson CD, Lowy DR, Schiller JT. Interferon gamma prevents infectious entry of human papillomavirus 16 via an L2-dependent mechanism. *J Virol* 2017;91:e00168-17–00168117.
34. Habiger C, Jäger G, Walter M, Iftner T, Stubenrauch F. Interferon kappa inhibits human papillomavirus 31 transcription by inducing Sp100 proteins. *J Virol* 2015;90:694–704.
35. Dittmann M, Hoffmann HH, Scull MA, Gilmore RH, Bell KL *et al.* A serpin shapes the extracellular environment to prevent influenza A virus maturation. *Cell* 2015;160:631–643.
36. Barr BB, Benton EC, Mclaren K, Bunney MH, Smith IW *et al.* Papillomavirus infection and skin cancer in renal allograft recipients. *Lancet* 1989;2:224–225.
37. Billingsley ML, Yun J, Reese BE, Davidson CE, Buck-Koehntop BA *et al.* Functional and structural properties of stannin: roles in cellular growth, selective toxicity, and mitochondrial responses to injury. *J Cell Biochem* 2006;98:243–250.
38. Toggas SM, Krady JK, Billingsley ML. Molecular neurotoxicology of trimethyltin: identification of stannin, a novel protein expressed in trimethyltin-sensitive cells. *Mol Pharmacol* 1992;42:44–56.
39. The Human Protein Atlas. www.proteinatlas.org/ENSG00000184602-SNN/tissue/cervix%2C+uterine.
40. Fagerberg L, Hallstrom BJ, Lindskog C, Uhlen M *et al.* Tissue-based map of the human proteome. *Science* 2015;347:12604191–12604199.
41. Griffin LM, Cicchini L, Pyeon D. Human papillomavirus infection is inhibited by host autophagy in primary human keratinocytes. *Virology* 2013;437:12–19.
42. Surviladze Z, Sterk RT, Deharo SA, Ozbun MA. Cellular entry of human papillomavirus type 16 involves activation of the phosphatidylinositol 3-kinase/Akt/mTOR pathway and inhibition of autophagy. *J Virol* 2013;87:2508–2517.
43. Pyo JO, Jang MH, Kwon YK, Lee HJ, Jun JI *et al.* Essential roles of Atg5 and FADD in autophagic cell death: dissection of autophagic

cell death into vacuole formation and cell death. *J Biol Chem* 2005;280:20722–20729.

44. **Reese BE, Krissinger D, Yun JK, Billingsley ML.** Elucidation of stannin function using microarray analysis: implications for cell cycle control. *Gene Expr* 2006;13:41–52.
45. **Bronnimann MP, Calton CM, Chiquette SF, Li S, Lu M *et al.*** Furin cleavage of L2 during papillomavirus infection: minimal dependence on cyclophilins. *J Virol* 2016;90:6224–6234.
46. **Ishii Y, Tanaka K, Kondo K, Takeuchi T, Mori S *et al.*** Inhibition of nuclear entry of HPV16 pseudovirus-packaged DNA by an anti-HPV16 L2 neutralizing antibody. *Virology* 2010;406:181–188.
47. **Leifer CA, Kennedy MN, Mazzoni A, Lee C, Kruhlak MJ *et al.*** TLR9 is localized in the endoplasmic reticulum prior to stimulation. *J Immunol* 2004;173:1179–1183.
48. **Sapp M, Kraus U, Volpers C, Snijders PJ, Walboomers JM *et al.*** Analysis of type-restricted and cross-reactive epitopes on virus-like particles of human papillomavirus type 33 and in infected tissues using monoclonal antibodies to the major capsid protein. *J Gen Virol* 1994;75:3375–3383.
49. **Söderberg O, Gullberg M, Jarvius M, Ridderstråle K, Leuchowius KJ *et al.*** Direct observation of individual endogenous protein complexes in situ by proximity ligation. *Nat Methods* 2006;3:995–1000.
50. **Lipovsky A, Zhang W, Iwasaki A, DiMaio D.** Application of the proximity-dependent assay and fluorescence imaging approaches to study viral entry pathways. *Methods Mol Biol* 2015;1270:437–451.
51. **Daulat AM, Maurice P, Froment C, Guillaume JL, Broussard C *et al.*** Purification and identification of G protein-coupled receptor protein complexes under native conditions. *Mol Cell Proteomics* 2007;6:835–844.
52. **Chinnapen DJ, Chinnapen H, Saslowsky D, Lencer WI.** Rafting with cholera toxin: endocytosis and trafficking from plasma membrane to ER. *FEMS Microbiol Lett* 2007;266:129–137.
53. **Seaman MN.** Cargo-selective endosomal sorting for retrieval to the Golgi requires retromer. *J Cell Biol* 2004;165:111–122.
54. **Schoggins JW, Macduff DA, Imanaka N, Gainey MD, Shrestha B *et al.*** Pan-viral specificity of IFN-induced genes reveals new roles for cGAS in innate immunity. *Nature* 2014;505:691–695.
55. **Molejon MI, Ropolo A, Re AL, Boggio V, Vaccaro MI.** The VMP1-Beclin 1 interaction regulates autophagy induction. *Sci Rep* 2013;3:1055.
56. **Sapp MJ.** HPV virions hitchhike a ride on retromer complexes. *Proc Natl Acad Sci USA* 2013;110:7116–7117.
57. **Zhang J, Reiling C, Reinecke JB, Prislan I, Marky LA *et al.*** Rabankyrin-5 interacts with EHD1 and Vps26 to regulate endocytic trafficking and retromer function. *Traffic* 2012;13:745–757.
58. **DiGiuseppe S, Bienkowska-Haba M, Guion LGM, Keiffer TR, Sapp M.** Human papillomavirus major capsid protein L1 remains associated with the incoming viral genome throughout the entry process. *J Virol* 2017:e00537-17.
59. **Wiens ME, Smith JG.** α-defensin HD5 inhibits human papillomavirus 16 infection via capsid stabilization and redirection to the lysosome. *MBio* 2017;8:e02304-16.
60. **Griffin LM, Cicchini L, Xu T, Pyeon D.** Human keratinocyte cultures in the investigation of early steps of human papillomavirus infection. *Methods Mol Biol* 2014;1195:219–238.
61. **Goodwin EC, Yang E, Lee CJ, Lee HW, DiMaio D *et al.*** Rapid induction of senescence in human cervical carcinoma cells. *Proc Natl Acad Sci USA* 2000;97:10978–10983.
62. **Desai P, Person S.** Incorporation of the green fluorescent protein into the herpes simplex virus type 1 capsid. *J Virol* 1998;72:7563–7568.